Modeling of Rheological Object with Square or Cubic Finite Element

Zhongkui Wang, Shinichi Hirai
Ritsumeikan University/Department of Robotics, Kusatsu, Japan

***Abstract*— Rheological object, such as various food products and biological tissues, has both elastic and plastic properties. Modeling of rheological object has not been studied frequently comparing with the modeling of elastic one. Our previously developed FE models of rheological objects were based on triangular or tetrahedra finite elements. In this paper, the FE model of rheological object formulated with square (2D) or cubic (3D) finite elements were presented. At first, the 2D FE model with square elements was formulated and was then extended to 3D case with cubic elements. The developed FE models were then utilized to simulate regular shaped objects and computation cost and simulation results were compared with the results from triangular- or tetrahedra- based models. We found that the FE model with square or cubic elements works as well as the model based on triangular or tetrahedra elements but can save computation cost with a speed-up ratio of about 30% in 2D or 50% in 3D cases.**

I. INTRODUCTION

In our living life, we can find many rheological objects, such as various food products, biological organs and tissues. Different from elastic object, rheological object always yield residual deformation after a loading-unloading operation. This makes it more difficult to model a rheological object than an elastic one. In medical related applications, elastic objects have been modeled frequently since most researchers assumed that the biological organs and tissues are totally recoverable from the deformation or they only care about the deformation during but not after the operation. However, some biological tissues, such as brain, demonstrate rheological behaviors under certain operation [1]. Residual deformation also happens in some dropsical organs or tissues during a period of time after an operation and it may be very important for diagnosis of diseases. Such rheological behaviors cannot be simulated using elastic models and have to be simulated using rheological models. Besides, many other objects, such as various food products, demonstrate rheological behaviors under loading-unloading operations. Unfortunately, modeling and simulation of rheological object has not been studied frequently so far.

Early work on modeling rheological object dates back to Terzopoulos *et al*. [2], who proposed a Burger model to describe rheological behaviors. Unfortunately, it is only a conceptual description and no simulation results were given. Two-layered Maxwell model [3] has been used to simulate rheological forces when a sushi was grasped by a robot hand. Good agreements in forces between simulation and experimental results were obtained. However, the model is limited to one-dimensional (1D) simulation. In two-dimensional (2D) and three-dimensional (3D) simulations, two popular modeling methods are frequently employed. One is Mass-Spring-Damper (MSD) model and the other one is Finite Element (FE) model. A MSD model consists of a mesh of mass points connected between each other by a series of links. The dynamic behaviors of each link are governed by several springs and dampers connected in certain configuration [4]. On the other hand, in FE model an object is described by a set of finite elements (*e.g.*, triangles and tetrahedra in 2D and 3D cases, respectively). Dynamic behaviors of the object are then described by the behaviors of individual elements. MSD model has been utilized to model a food dough, typical rheological object, by Noborio *et al*. They investigated three different mesh configurations: the lattice [5], the truss [6], and the hierarchical structures [7], with decreased MSD elements in order to reduce the computation cost. The MSD model has advantages of simple formulation and relatively low computation cost, but the formulation is not based on continuum mechanics and the geometrical topology significantly affects the simulation results. In our previous works, we have developed FE dynamic models for simulating rheological objects and proposed optimization-based methods for estimating physical parameters [8], [9], [10]. We have also developed an FE contact model to simulate the interactions between two objects [11]. To simulate large deformation and deformation with rotation motion, nonlinear Green strain tensor has also been introduced into our FE model [12].

Our previous FE models were formulated with 2D triangular and 3D tetrahedra finite elements, which are the most popular and elementary elements. However in FE method, other elements are also available, such as 2D quadrilateral and 3D hexahedron elements, etc. In this paper, therefore, the formulation of FE rheological model with 2D square and 3D cubic finite elements will be formulated and the comparisons in computation cost and simulation results with previously triangular/tetrahedra elements will be performed.

The rest of the paper is organized as follows. Section 2 presents the formulation of 2D model with square finite elements. 3D model with cubic elements will be presented in Section 3. Section 4 demonstrates computation costs and simulation results of models with square/cubic and triangle/tetrahedra finite elements and comparisons and discussions will be made. The conclusions and future works given in Section 5.

II. 2D MODEL WITH SQUARE FINITE ELEMENT

A. Formulation of Elastic Force

First of all, let us start with 2D modeling of elastic deformation with square finite element. Let $\square P_i P_j P_k P_l$ be a square

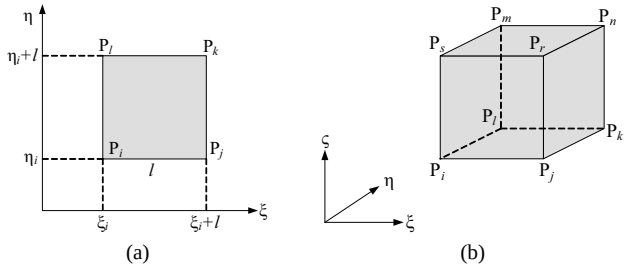

Fig. 1: Square (a) and cubic (b) finite element.

element with the side length l, as shown in Fig. 1a. Assume that $\mathrm{P}_i\mathrm{P}_j$ is parallel to ξ-axis and $\mathrm{P}_i\mathrm{P}_l$ is parallel to η-axis. Let (ξ_i,η_i) be the coordinates of point P_i. Then, coordinates of P_j, P_k, and P_l can be calculated easily. Let us define shape functions corresponding to P_i, P_j, P_k, and P_l as

$$\begin{aligned} N_{i,j,k,l} &= \frac{(\xi_i+l-\xi)(\eta_i+l-\eta)}{l^2}, \quad N_{j,k,l,i} = \frac{(\xi-\xi_i)(\eta_i+l-\eta)}{l^2}, \\ N_{k,l,i,j} &= \frac{(\xi-\xi_i)(\eta-\eta_i)}{l^2}, \quad N_{l,i,j,k} = \frac{(\xi_i+l-\xi)(\eta-\eta_i)}{l^2}, \end{aligned} \tag{1}$$

where $\boldsymbol{\xi} = [\xi,\eta]^{\mathrm{T}}$ is any point inside square $\square\mathrm{P}_i\mathrm{P}_j\mathrm{P}_k\mathrm{P}_l$. Let $\boldsymbol{u} = [u(\xi,\eta), v(\xi,\eta)]^{\mathrm{T}}$ be displacement vector of the point. The displacement vector can be then approximated using the shape functions as:

$$\boldsymbol{u} = \boldsymbol{u}_i N_{i,j,k,l} + \boldsymbol{u}_j N_{j,k,l,i} + \boldsymbol{u}_k N_{k,l,i,j} + \boldsymbol{u}_l N_{l,i,j,k}, \tag{2}$$

where $\boldsymbol{u}_i$, $\boldsymbol{u}_j$, $\boldsymbol{u}_k$, and $\boldsymbol{u}_l$ be displacement vectors at nodal points P_i, P_j, P_k, and P_l, respectively. Let $\boldsymbol{u}_{i,j,k,l} = [\boldsymbol{u}_i,\boldsymbol{u}_j,\boldsymbol{u}_k,\boldsymbol{u}_l]^{\mathrm{T}}$ be a collective vector consisting of displacements at P_i, P_j, P_k, and P_l. We also introduce another two collective vectors as: $\boldsymbol{\gamma}_u = [u_i,u_j,u_k,u_l]^{\mathrm{T}}$ and $\boldsymbol{\gamma}_v = [v_i,v_j,v_k,v_l]^{\mathrm{T}}$.

Let us calculate strain vector inside $\square\mathrm{P}_i\mathrm{P}_j\mathrm{P}_k\mathrm{P}_l$. For an isotropic linear material, the Cauchy strain tensor $\boldsymbol{\varepsilon} = [\varepsilon_{\xi\xi},\varepsilon_{\eta\eta},2\varepsilon_{\xi\eta}]^{\mathrm{T}}$ is formulated as

$$\begin{aligned} \varepsilon_{\xi\xi} &= \frac{\partial u}{\partial \xi} = \boldsymbol{a}^{\mathrm{T}}\boldsymbol{\gamma}_u, \\ \varepsilon_{\eta\eta} &= \frac{\partial v}{\partial \eta} = \boldsymbol{b}^{\mathrm{T}}\boldsymbol{\gamma}_v, \\ 2\varepsilon_{\xi\eta} &= \frac{\partial u}{\partial \eta} + \frac{\partial v}{\partial \xi} = \boldsymbol{b}^{\mathrm{T}}\boldsymbol{\gamma}_u + \boldsymbol{a}^{\mathrm{T}}\boldsymbol{\gamma}_v, \end{aligned} \tag{3}$$

where

$$\boldsymbol{a} = \frac{1}{l^2}\begin{bmatrix} -(\eta_i+l-\eta) \\ (\eta_i+l-\eta) \\ (\eta-\eta_i) \\ -(\eta-\eta_i) \end{bmatrix}, \quad \boldsymbol{b} = \frac{1}{l^2}\begin{bmatrix} -(\xi_i+l-\xi) \\ -(\xi-\xi_i) \\ (\xi-\xi_i) \\ (\xi_i+l-\xi) \end{bmatrix}. \tag{4}$$

Note that the density of elastic potential energy of an isotropic linear material can be formulated as

$$W = \frac{1}{2}\lambda(\varepsilon_{\xi\xi}+\varepsilon_{\eta\eta})^2 + \frac{1}{2}\mu[2\varepsilon_{\xi\xi}^2 + 2\varepsilon_{\eta\eta}^2 + (2\varepsilon_{\xi\eta})^2], \tag{5}$$

where scalars λ and μ denote Lamé's constants, which can be calculated by Young's modulus E and Poisson's ratio γ as follows:

$$\lambda = \frac{\gamma E}{(1+\gamma)(1-2\gamma)}, \qquad \mu = \frac{E}{2(1+\gamma)}. \tag{6}$$

Integrating the energy density Eq. 5 over the square element $\square\mathrm{P}_i\mathrm{P}_j\mathrm{P}_k\mathrm{P}_l$ yields the potential energy stored in the element. Note that

$$\begin{aligned} G^\lambda &\triangleq \frac{1}{2}\int_\square (\varepsilon_{\xi\xi}+\varepsilon_{\eta\eta})^2 h\,\mathrm{d}S \\ &= \frac{1}{2}\begin{bmatrix}\boldsymbol{\gamma}_u^{\mathrm{T}} & \boldsymbol{\gamma}_v^{\mathrm{T}}\end{bmatrix}\begin{bmatrix}\boldsymbol{L}_{aa} & \boldsymbol{L}_{ab} \\ \boldsymbol{L}_{ba} & \boldsymbol{L}_{bb}\end{bmatrix}\begin{bmatrix}\boldsymbol{\gamma}_u \\ \boldsymbol{\gamma}_v\end{bmatrix}, \end{aligned} \tag{7}$$

where h denotes the thickness of the square element and constant coefficient matrices are formulated as

$$\begin{aligned} \boldsymbol{L}_{aa} &= \int_\square \boldsymbol{a}\boldsymbol{a}^{\mathrm{T}} h\,\mathrm{d}S, \quad \boldsymbol{L}_{bb} = \int_\square \boldsymbol{b}\boldsymbol{b}^{\mathrm{T}} h\,\mathrm{d}S, \\ \boldsymbol{L}_{ab} &= \boldsymbol{L}_{ba} = \int_\square \boldsymbol{a}\boldsymbol{b}^{\mathrm{T}} h\,\mathrm{d}S. \end{aligned} \tag{8}$$

Similarly, we also have

$$\begin{aligned} G^\mu &\triangleq \int_\square (\varepsilon_{\xi\xi}^2+\varepsilon_{\eta\eta}^2) h\,\mathrm{d}S + \frac{1}{2}\int_\square (2\varepsilon_{\xi\eta})^2 h\,\mathrm{d}S \\ &= \frac{1}{2}\begin{bmatrix}\boldsymbol{\gamma}_u^{\mathrm{T}} & \boldsymbol{\gamma}_v^{\mathrm{T}}\end{bmatrix}\begin{bmatrix}\boldsymbol{M}_{aa} & \boldsymbol{M}_{ab} \\ \boldsymbol{M}_{ba} & \boldsymbol{M}_{bb}\end{bmatrix}\begin{bmatrix}\boldsymbol{\gamma}_u \\ \boldsymbol{\gamma}_v\end{bmatrix}, \end{aligned} \tag{9}$$

where constant coefficient matrices are formulated as

$$\begin{aligned} &\boldsymbol{M}_{aa} = 2\boldsymbol{L}_{aa} + \boldsymbol{L}_{bb}, \quad \boldsymbol{M}_{bb} = 2\boldsymbol{L}_{bb} + \boldsymbol{L}_{aa}, \\ &\boldsymbol{M}_{ab} = \boldsymbol{L}_{ba}, \quad \boldsymbol{M}_{ba} = \boldsymbol{L}_{ab}. \end{aligned} \tag{10}$$

Consequently, potential energy stored in the square element is calculated as

$$U_{i,j,k,l} = \lambda G^\lambda + \mu G^\mu. \tag{11}$$

Partial derivative of integral G^λ with respect to $\boldsymbol{\gamma} = [\boldsymbol{\gamma}_u^{\mathrm{T}},\boldsymbol{\gamma}_v^{\mathrm{T}}]^{\mathrm{T}}$ is formulated as

$$\frac{\partial G^\lambda}{\partial \boldsymbol{\gamma}} = \begin{bmatrix}\boldsymbol{L}_{aa} & \boldsymbol{L}_{ab} \\ \boldsymbol{L}_{ba} & \boldsymbol{L}_{bb}\end{bmatrix}\begin{bmatrix}\boldsymbol{\gamma}_u \\ \boldsymbol{\gamma}_v\end{bmatrix}, \tag{12}$$

Similarly, we have

$$\frac{\partial G^\mu}{\partial \boldsymbol{\gamma}} = \begin{bmatrix}\boldsymbol{M}_{aa} & \boldsymbol{M}_{ab} \\ \boldsymbol{M}_{ba} & \boldsymbol{M}_{bb}\end{bmatrix}\begin{bmatrix}\boldsymbol{\gamma}_u \\ \boldsymbol{\gamma}_v\end{bmatrix}, \tag{13}$$

Note that the following permutation converts vector $\boldsymbol{\gamma}$ into $\boldsymbol{u}_{i,j,k,l}$:

$$\boldsymbol{P} = \begin{pmatrix} u_i & u_j & u_k & u_l & v_i & v_j & v_k & v_l \\ u_i & v_i & u_j & v_j & u_k & v_k & u_l & v_l \end{pmatrix}. \tag{14}$$

This permutation converts $\partial G^\lambda/\partial\boldsymbol{\gamma}$ into $\partial G^\lambda/\partial\boldsymbol{u}_{i,j,k,l}$ and $\partial G^\mu/\partial\boldsymbol{\gamma}$ into $\partial G^\mu/\partial\boldsymbol{u}_{i,j,k,l}$. As a result, a set of nodal forces generated on P_i through P_l can be formulated as follows:

$$\begin{aligned} \boldsymbol{f}_{i,j,k,l} &= -\frac{\partial U_{i,j,k,l}}{\partial \boldsymbol{u}_{i,j,k,l}} = -\left(\lambda\frac{\partial G^\lambda}{\partial \boldsymbol{u}_{i,j,k,l}} + \mu\frac{\partial G^\mu}{\partial \boldsymbol{u}_{i,j,k,l}}\right) \\ &= -\left(\lambda\boldsymbol{J}_\square^\lambda + \mu\boldsymbol{J}_\square^\mu\right)\boldsymbol{u}_{i,j,k,l}. \end{aligned} \tag{15}$$

Note that $\boldsymbol{J}_\square^\lambda$ and $\boldsymbol{J}_\square^\mu$ are independent of ξ_i and η_i, or l. Namely, $\boldsymbol{K}_\square = \lambda\boldsymbol{J}_\square^\lambda + \mu\boldsymbol{J}_\square^\mu$ is a constant matrix and independent of nodal points coordinates. This is different from the FE model formulated with triangular element, in which connection matrices $\boldsymbol{J}_\lambda$ and $\boldsymbol{J}_\mu$ depend on the coordinates of nodal points [12].

Equation 15 is used to calculate the elastic forces generated on a square element $\square P_i P_j P_k P_l$. Summing up all forces generated on individual nodes, we are able to compute the elastic forces at all nodes as

$$\boldsymbol{F} = -\left(\lambda \boldsymbol{J}_{2D}^{\lambda} + \mu \boldsymbol{J}_{2D}^{\mu}\right) \boldsymbol{u}_N, \tag{16}$$

where $\boldsymbol{F}$ and $\boldsymbol{u}_N$ are force and displacement vectors of all nodes, matrices $\boldsymbol{J}_{2D}^{\lambda}$ and $\boldsymbol{J}_{2D}^{\mu}$ are referred as connection matrices and they can be calculated by summing up the contributions of $\boldsymbol{J}_{\square}^{\lambda}$ and $\boldsymbol{J}_{\square}^{\mu}$ from individual square elements.

B. Formulation of Rheological Force

A parallel five-element model (Fig. 1c in [12]) is employed in this paper to govern rheological behaviors of individual square elements. The constitutive law of this model is formulated as

$$\begin{aligned} &\dot{\sigma}_1 + \frac{E_1}{c_1}\sigma_1 = E_1\dot{\varepsilon}, \\ &\dot{\sigma}_2 + \frac{E_2}{c_2}\sigma_2 = E_2\dot{\varepsilon}, \\ &\sigma_3 = c_3\dot{\varepsilon}, \\ &\sigma = \sigma_1 + \sigma_2 + \sigma_3, \end{aligned} \tag{17}$$

where σ_1, σ_2, and σ_3 are stress at the first, second, and third layer of the five-element model, σ and ε are the stress and strain at the model, E_1, E_2, c_1, c_2, and c_3 are Young's moduli and viscous moduli of individual elastic and viscous elements of the model, respectively.

As presented in [12], the constitutive law Eq. 17 can be converted into a relationship between rheological force and displacement by performing a series of replacements based on the formulation of elastic force (Eq. 16) as

$$\begin{aligned} &\dot{\boldsymbol{F}}_1 + \frac{E_1}{c_1}\boldsymbol{F}_1 = \left(\lambda_1^{ela}\boldsymbol{J}_{2D}^{\lambda} + \mu_1^{ela}\boldsymbol{J}_{2D}^{\mu}\right)\dot{\boldsymbol{u}}_N, \\ &\dot{\boldsymbol{F}}_2 + \frac{E_2}{c_2}\boldsymbol{F}_2 = \left(\lambda_2^{ela}\boldsymbol{J}_{2D}^{\lambda} + \mu_2^{ela}\boldsymbol{J}_{2D}^{\mu}\right)\dot{\boldsymbol{u}}_N, \\ &\boldsymbol{F}_3 = \left(\lambda_3^{vis}\boldsymbol{J}_{2D}^{\lambda} + \mu_3^{vis}\boldsymbol{J}_{2D}^{\mu}\right)\dot{\boldsymbol{u}}_N, \\ &\boldsymbol{F}_{2D}^{rheo} = \boldsymbol{F}_1 + \boldsymbol{F}_2 + \boldsymbol{F}_3, \end{aligned} \tag{18}$$

where $\boldsymbol{F}_1$, $\boldsymbol{F}_2$, and $\boldsymbol{F}_3$ are force vectors corresponding to stress σ_1, σ_2, and σ_3, respectively, λ_1^{ela}, μ_1^{ela}, λ_2^{ela}, and μ_2^{ela} are Lamé constants corresponding to E_1 and E_2 and can be calculated by Eq. 3 of [12], λ_3^{vis} and μ_3^{vis} described the model's viscosity and are defined by Eq. 15 of [12], vectors $\boldsymbol{u}_N$ and $\boldsymbol{F}_{2D}^{rheo}$ denote the rheological displacement and force vectors generated on the FE model.

C. Dynamic Equations of Rheological Deformation

After having the formulation (Eq. 18) of rheological force, we can formulate a set of dynamic equations of rheological deformation. At first, let us compute the kinetic energy inside square element $\square P_i P_j P_k P_l$. Note that the rate of displacement vector with respect to time is described by

$$\dot{\boldsymbol{u}} = \dot{\boldsymbol{u}}_i N_{i,j,k,l} + \dot{\boldsymbol{u}}_j N_{j,k,l,i} + \dot{\boldsymbol{u}}_k N_{k,l,i,j} + \dot{\boldsymbol{u}}_l N_{l,i,j,k}, \tag{19}$$

at any point inside the element. Kinetic energy of the element is then described as:

$$T_{i,j,k,l} = \int_{\square P_i P_j P_k P_l} \frac{1}{2}\rho \dot{\boldsymbol{u}}^{\mathrm{T}}\dot{\boldsymbol{u}} h \,\mathrm{d}S, \tag{20}$$

where ρ denotes the density of the material. Substituting Eq. 19 into Eq. 20 and integrating it, we have

$$T_{i,j,k,l} = \frac{1}{2}\dot{\boldsymbol{u}}_{i,j,k,l}^{\mathrm{T}}\boldsymbol{M}_{i,j,k,l}\dot{\boldsymbol{u}}_{i,j,k,l}, \tag{21}$$

where

$$\boldsymbol{M}_{i,j,k,l} = \frac{\rho l^2 h}{36}\begin{bmatrix} 4\boldsymbol{I}_{2\times2} & 2\boldsymbol{I}_{2\times2} & \boldsymbol{I}_{2\times2} & 2\boldsymbol{I}_{2\times2} \\ 2\boldsymbol{I}_{2\times2} & 4\boldsymbol{I}_{2\times2} & 2\boldsymbol{I}_{2\times2} & \boldsymbol{I}_{2\times2} \\ \boldsymbol{I}_{2\times2} & 2\boldsymbol{I}_{2\times2} & 4\boldsymbol{I}_{2\times2} & 2\boldsymbol{I}_{2\times2} \\ 2\boldsymbol{I}_{2\times2} & \boldsymbol{I}_{2\times2} & 2\boldsymbol{I}_{2\times2} & 4\boldsymbol{I}_{2\times2} \end{bmatrix} \tag{22}$$

with $\boldsymbol{I}_{2\times2}$ be a 2×2 unit matrix. Note that the summation of all blocks of matrix $\boldsymbol{M}_{i,j,k,l}$ is equal to $\rho l^2 h \boldsymbol{I}_{2\times2}$, which is the mass of square element $\square P_i P_j P_k P_l$. The mass matrix $\boldsymbol{M}$ of an object with square mesh can be then calculated by summing up the contributions of $\boldsymbol{M}_{i,j,k,l}$ from individual square elements.

Assuming that a rheological object is fixed on ground and the top surface of the object is pushed down with a displacement function of $d(t)$. Both geometric constraints on the nodes of bottom and top surfaces can be described by $\boldsymbol{A}^{\mathrm{T}}\boldsymbol{u}_N$ and $\boldsymbol{B}^{\mathrm{T}}\boldsymbol{u}_N$ with matrices $\boldsymbol{A}$ and $\boldsymbol{B}$ denoting the nodes to be constrained. Thus, Lagrange equation under these two geometric constraints can be formulated as

$$L = \frac{1}{2}\dot{\boldsymbol{u}}_N^{\mathrm{T}}\boldsymbol{M}\dot{\boldsymbol{u}}_N - U + \boldsymbol{\lambda}_1^{\mathrm{T}}\boldsymbol{A}^{\mathrm{T}}\boldsymbol{u}_N + \boldsymbol{\lambda}_2^{\mathrm{T}}\boldsymbol{B}^{\mathrm{T}}\boldsymbol{u}_N, \tag{23}$$

where $\boldsymbol{\lambda}_1$ and $\boldsymbol{\lambda}_2$ are Lagrange multipliers denoting a set of constraint forces, scalar U denotes the potential energy generated inside the object and can be calculated by summing up the contributions of Eq. 11 from individual elements. Note that the partial derivative of U with respect to $\boldsymbol{u}_N$ yields the force vector generated on all nodes.

Applying Lagrange equations of motion to Eq. 23, a set of motion equations of nodes can be formulated as

$$-\boldsymbol{F}_{2D}^{rheo} + \boldsymbol{A}\boldsymbol{\lambda}_1 + \boldsymbol{B}\boldsymbol{\lambda}_2 - \boldsymbol{M}\ddot{\boldsymbol{u}}_N = 0. \tag{24}$$

Using the Constraint Stabilization Method (CSM) [13] to convert a set of geometric constraints $\boldsymbol{A}^{\mathrm{T}}\boldsymbol{u}_N = 0$ and $\boldsymbol{B}^{\mathrm{T}}\boldsymbol{u}_N = 0$ into a set of differential equations, we have

$$\begin{aligned} \boldsymbol{A}^{\mathrm{T}}\ddot{\boldsymbol{u}}_N + \boldsymbol{A}^{\mathrm{T}}\left(2\omega\dot{\boldsymbol{u}}_N + \omega^2\boldsymbol{u}_N\right) = 0, \\ \boldsymbol{B}^{\mathrm{T}}\left(\ddot{\boldsymbol{u}}_N - \ddot{\boldsymbol{d}}\right) + \boldsymbol{B}^{\mathrm{T}}\left[2\omega\left(\dot{\boldsymbol{u}}_N - \dot{\boldsymbol{d}}\right) + \omega^2\left(\boldsymbol{u}_N - \boldsymbol{d}\right)\right] = 0, \end{aligned} \tag{25}$$

where ω is a predetermined angular frequency and is set to 1000 for both constraints during simulation.

Introducing velocity vector $\boldsymbol{v}_N = \dot{\boldsymbol{u}}_N$ and combining Eqs. 18, 24, and 25, we obtain a set of differential equations which formulated 2D FE model of rheological deformation. Numerically solving these differential equations, we are able to compute the rheological force and deformation based on square finite elements.

III. 3D Model with Cubic Elements

In 3D case, we formulate the FE modeling with cubic elements, as shown in Fig. 1b. The formulation process is the same with 2D square case. Some variables, however, have to be reformulated to fit the 3D coordinate system. First of all, the shape functions are defined as

$$\begin{aligned}
N_i &= \frac{1}{l^3}(\xi_i + l - \xi)(\eta_i + l - \eta)(\zeta_i + l - \zeta),\\
N_j &= \frac{1}{l^3}(\xi - \xi_i)(\eta_i + l - \eta)(\zeta_i + l - \zeta),\\
N_k &= \frac{1}{l^3}(\xi - \xi_i)(\eta - \eta_i)(\zeta_i + l - \zeta),\\
N_l &= \frac{1}{l^3}(\xi_i + l - \xi)(\eta - \eta_i)(\zeta_i + l - \zeta),\\
N_m &= \frac{1}{l^3}(\xi_i + l - \xi)(\eta - \eta_i)(\zeta - \zeta_i),\\
N_n &= \frac{1}{l^3}(\xi - \xi_i)(\eta - \eta_i)(\zeta - \zeta_i),\\
N_r &= \frac{1}{l^3}(\xi - \xi_i)(\eta_i + l - \eta)(\zeta - \zeta_i),\\
N_s &= \frac{1}{l^3}(\xi_i + l - \xi)(\eta_i + l - \eta)(\zeta - \zeta_i),
\end{aligned} \tag{26}$$

where (ξ_i, η_i, ζ_i) is the coordinate of point P_i, $[\xi, \eta, \zeta]^{\mathrm{T}}$ denotes any point inside the cubic element $\boxdot \mathrm{P}_i\mathrm{P}_j\mathrm{P}_k\mathrm{P}_l\mathrm{P}_m\mathrm{P}_n\mathrm{P}_r\mathrm{P}_s$, l is the side length of the element.

Two components of elastic potential energy are recomputed as

$$\begin{aligned}
G_{3D}^{\lambda} &\triangleq \frac{1}{2}\int_{\boxdot} \left(\varepsilon_{\xi\xi} + \varepsilon_{\eta\eta} + \varepsilon_{\zeta\zeta}\right)^2 \mathrm{d}V,\\
G_{3D}^{\mu} &\triangleq \int_{\boxdot} \left(\varepsilon_{\xi\xi}^2 + \varepsilon_{\eta\eta}^2 + \varepsilon_{\zeta\zeta}^2\right) \mathrm{d}V\\
&\quad + \frac{1}{2}\int_{\boxdot} \left[\left(2\varepsilon_{\eta\zeta}\right)^2 + \left(2\varepsilon_{\zeta\xi}\right)^2 + \left(2\varepsilon_{\xi\eta}\right)^2\right] \mathrm{d}V,
\end{aligned} \tag{27}$$

where $\varepsilon_{\xi\xi}$, $\varepsilon_{\eta\eta}$, $\varepsilon_{\zeta\zeta}$, $\varepsilon_{\xi\eta}$, $\varepsilon_{\eta\zeta}$, and $\varepsilon_{\zeta\xi}$ can be calculated from the linear Cauchy strain tensor in 3D case.

Taking the partial derivative of the above integrals G_{3D}^{λ} and G_{3D}^{μ} with respect to $\boldsymbol{u}_{\boxdot}$, we have a set of nodal forces generated on P_i through P_s as:

$$\boldsymbol{f}_{\boxdot} = -\left(\lambda \boldsymbol{J}_{\boxdot}^{\lambda} + \mu \boldsymbol{J}_{\boxdot}^{\mu}\right)\boldsymbol{u}_{\boxdot}. \tag{28}$$

where $\boldsymbol{f}_{\boxdot}$ and $\boldsymbol{u}_{\boxdot}$ denote the force and displacement vectors at nodes of the cubic element $\boxdot$, matrices $\boldsymbol{J}_{\boxdot}^{\lambda}$ and $\boldsymbol{J}_{\boxdot}^{\mu}$ are constant matrices with a dimension of 24×24. By summing up the contributions of $\boldsymbol{J}_{\boxdot}^{\lambda}$ and $\boldsymbol{J}_{\boxdot}^{\mu}$ from individual cubic elements, we are able to calculate a stiffness matrix $\boldsymbol{K}_{3D} = \lambda \boldsymbol{J}_{3D}^{\lambda} + \mu \boldsymbol{J}_{3D}^{\mu}$ for an object. The dimension of matrices $\boldsymbol{J}_{3D}^{\lambda}$ and $\boldsymbol{J}_{3D}^{\mu}$ is $3N \times 3N$ with N denoting the nodal number of the mesh. By replacing $\boldsymbol{J}_{2D}^{\lambda}$ by $\boldsymbol{J}_{3D}^{\lambda}$ and $\boldsymbol{J}_{2D}^{\mu}$ by $\boldsymbol{J}_{3D}^{\mu}$ in Eq. 18, we are able to compute the rheological forces $\boldsymbol{F}_{3D}^{rheo}$ in 3D case. Consequently, we can formulate a set of dynamic equations of rheological deformation in 3D case as presented in the last section. Note that the mass matrix of a cubic element can be calculated as

$$\boldsymbol{M}_{\boxdot} = \frac{\rho l^3}{6^3}\begin{bmatrix}
8\boldsymbol{I}_3 & 4\boldsymbol{I}_3 & 2\boldsymbol{I}_3 & 4\boldsymbol{I}_3 & 2\boldsymbol{I}_3 & \boldsymbol{I}_3 & 2\boldsymbol{I}_3 & 4\boldsymbol{I}_3\\
4\boldsymbol{I}_3 & 8\boldsymbol{I}_3 & 4\boldsymbol{I}_3 & 2\boldsymbol{I}_3 & \boldsymbol{I}_3 & 2\boldsymbol{I}_3 & 4\boldsymbol{I}_3 & 2\boldsymbol{I}_3\\
2\boldsymbol{I}_3 & 4\boldsymbol{I}_3 & 8\boldsymbol{I}_3 & 4\boldsymbol{I}_3 & 2\boldsymbol{I}_3 & 4\boldsymbol{I}_3 & 2\boldsymbol{I}_3 & \boldsymbol{I}_3\\
4\boldsymbol{I}_3 & 2\boldsymbol{I}_3 & 4\boldsymbol{I}_3 & 8\boldsymbol{I}_3 & 4\boldsymbol{I}_3 & 2\boldsymbol{I}_3 & \boldsymbol{I}_3 & 2\boldsymbol{I}_3\\
2\boldsymbol{I}_3 & \boldsymbol{I}_3 & 2\boldsymbol{I}_3 & 4\boldsymbol{I}_3 & 8\boldsymbol{I}_3 & 4\boldsymbol{I}_3 & 2\boldsymbol{I}_3 & 4\boldsymbol{I}_3\\
\boldsymbol{I}_3 & 2\boldsymbol{I}_3 & 4\boldsymbol{I}_3 & 2\boldsymbol{I}_3 & 4\boldsymbol{I}_3 & 8\boldsymbol{I}_3 & 4\boldsymbol{I}_3 & 2\boldsymbol{I}_3\\
2\boldsymbol{I}_3 & 4\boldsymbol{I}_3 & 2\boldsymbol{I}_3 & \boldsymbol{I}_3 & 2\boldsymbol{I}_3 & 4\boldsymbol{I}_3 & 8\boldsymbol{I}_3 & 4\boldsymbol{I}_3\\
4\boldsymbol{I}_3 & 2\boldsymbol{I}_3 & \boldsymbol{I}_3 & 2\boldsymbol{I}_3 & 4\boldsymbol{I}_3 & 2\boldsymbol{I}_3 & 4\boldsymbol{I}_3 & 8\boldsymbol{I}_3
\end{bmatrix} \tag{29}$$

with $\boldsymbol{I}_3$ be a 3×3 unit matrix.

From the above formulation we found that the major difference in 2D and 3D model is the calculation of the connection and mass matrices. Fortunately, they are constant matrices and can be prepared in advance.

IV. Simulation and Comparison Results

A. Simulation Setup

2D and 3D FE simulations are performed with different meshes and in different nodal resolutions. Assuming a 2D regular-shaped object is fixed on ground with triangular and square meshes as shown in Fig. 2a and Fig. 2b, respectively. In 2D case, the nodal resolution of the object is set to 5×5. The top-center node is deformed vertically during simulation with a displacement function $d(t)$, which appears in Eq. 25 and is described by Fig. 2c. During time period $\left[0, t_{\mathrm{p}}\right]$, the object is pushed down with constant velocity and the time period is called push phase. During time period $\left[t_{\mathrm{p}}, t_{\mathrm{p}} + t_{\mathrm{k}}\right]$, the deformation generated in the object is kept unchange and it is called keep phase. Accordingly, the deformed shape in the keep phase is called keep-shape. After time $t_{\mathrm{p}} + t_{\mathrm{k}}$, the geometrical constraint on the top-center node is removed and the object is allowed to recover freely and finally reach a permanent shape, which is called final-shape accordingly. In 3D case, FE simulations with both tetrahedra and cubic meshes are performed and the same displacement function $d(t)$ is used to deform the object. Instead of pushing from the top-center node, the entire top surface of the object is deformed in 3D simulations. The size of the object is set to $0.08 \times 0.08\,\mathrm{mm}^2$ in 2D and $0.08 \times 0.08 \times 0.08\,\mathrm{mm}^3$ in 3D cases, respectively. The nodal resolutions used in simulations are set to 5×5 and 9×9 for 2D and $5 \times 5 \times 5$ and $9 \times 9 \times 9$ for 3D cases, respectively. The physical parameters used in simulations are the same and listed in Table I, where t_{sim} denotes total simulation time.

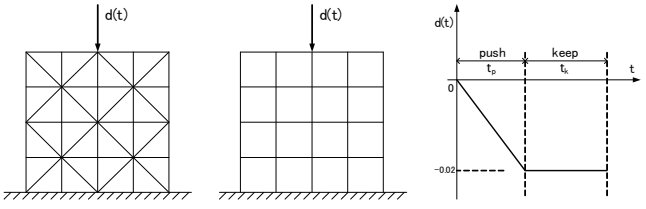

Fig. 2: A 2D regular-shaped object fixed on the ground with triangle (a) and square (b) mesh respectively, a displacement function $d(t)$ (c) is acted on the center node of the object.

TABLE I: Physical parameters used in simulations

Parameter	E_1 (Pa)	E_2 (Pa)	c_1 (Pa·s)	c_2 (Pa·s)	c_3 (Pa·s)
Value	1×10^4	2×10^4	3×10^6	2×10^5	1×10^2
Parameter	γ	h (m) 2D only	t_p (s)	t_k (s)	t_{sim} (s)
Value	0.35	0.012	2	4	10

B. Simulation Results and Comparisons

The simulations were coded by MATLAB's M-file and run on a desktop with an Intel CPU (2.8GHz) and 3.25 GB of RAM. The integrations were performed using a MATLAB's build-in function named "ode23". The computation costs of simulations were recorded and listed in Table II. We found that the element number of a square mesh is two times smaller than a triangular mesh in 2D case, but the speed-up ratio is about 30%. On the other hand, the element number of a cubic mesh is six times smaller than a tetrahedra mesh in 3D case, but the speed-up ratio is about 50%. We also found that the speed-up ratio is not increasing along with the increase of nodal resolutions. Therefore, we conclude that the square or cubic finite elements yield faster simulation comparing with the triangular or tetrahedra finite elements and the speed-up ratios are about 30% in 2D and 50% in 3D cases, respectively.

We also compared the simulation results of rheological forces and deformation from different meshes. Figure 3 shows the comparison results in 2D case with 5×5 and 9×9 nodal resolutions. We found that the deformed shapes from both meshes are almost same but a difference appears in rheological forces. The square mesh yields slightly smaller force than the triangular mesh. In other words, an object modeled by square mesh is slightly softer than the same object modeled by triangular mesh. In addition, we also found that larger nodal resolution yields smaller force amplitudes and better agreements in deformation. This tendency of force reduction will be weaker with the increase of the nodal resolution and finally becomes negligible as the nodal resolution reaches certain number [9].

TABLE II: Comparison of simulation costs

Model dim.	Nodal resol.	Element type	Element number	Sim. cost (s)	Speed-up ratio
2D	5×5	Triangle	32	8.66	32.33%
		Square	16	5.86	
	9×9	Triangle	128	42.92	31.78%
		Square	64	29.28	
3D	$5\times5\times5$	Tetrahedra	384	40.09	56.50%
		Cube	64	17.44	
	$9\times9\times9$	Tetrahedra	3072	8366.83	53.98%
		cube	512	3850.00	

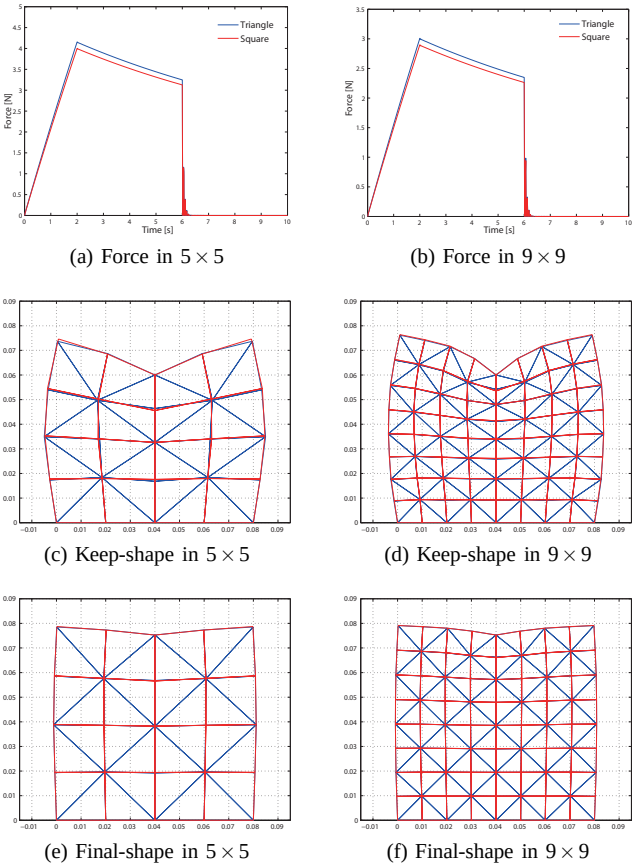

(a) Force in 5×5 (b) Force in 9×9

(c) Keep-shape in 5×5 (d) Keep-shape in 9×9

(e) Final-shape in 5×5 (f) Final-shape in 9×9

Fig. 3: Comparisons of simulation results in 2D with blue lines for triangular mesh and red lines for square mesh.

Comparison results in 3D case are shown in Fig. 4. For the convenience of clear comparison, only 2D projections of 3D deformation were given in the figure. From Fig. 4 we found that the deformation are matched very well but larger difference in forces appeared between both meshes. However, force trends of both meshes are same. The difference in forces between different meshes is caused by the geometrical topology. This difference can be eliminated by performing model calibration or parameter estimation. In other words, different FE meshes require different physical parameters in order to predict certain rheological force behaviors. The comparisons done in this paper tend to show that the square or cubic finite element has the same ability as the triangular or tetrahedra element for modeling rheological behaviors. In addition, 3D simulation snapshots of both resolutions are shown in Fig. 5 to demonstrate how 3D simulation is.

V. CONCLUSIONS AND FUTURE WORKS

In this paper, FE dynamic models of rheological objects were developed using 2D square and 3D cubic finite elements. Comparing with 2D triangular and 3D tetrahedra elements, the formulations with square and cubic elements are less

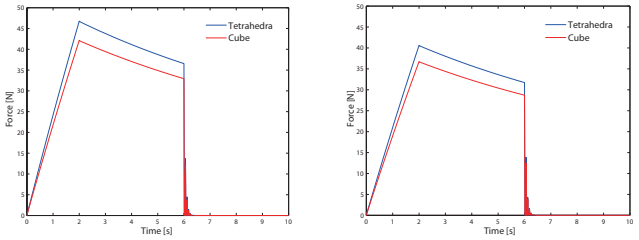

(a) Force in $5 \times 5 \times 5$ (b) Force in $9 \times 9 \times 9$

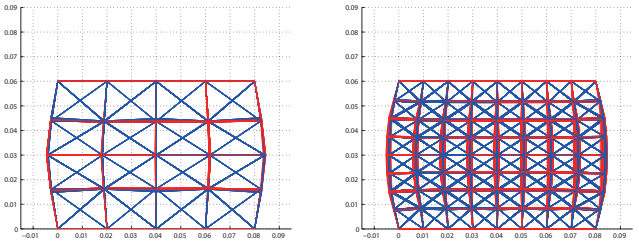

(c) Keep-shape in $5 \times 5 \times 5$ (d) Keep-shape in $9 \times 9 \times 9$

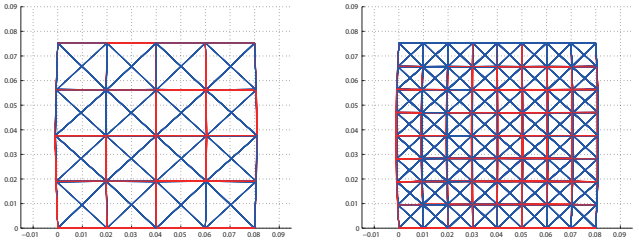

(e) Final-shape in $5 \times 5 \times 5$ (f) Final-shape in $9 \times 9 \times 9$

Fig. 4: Comparisons of simulation results in 3D with blue lines for tetrahedra mesh and red lines for cubic mesh.

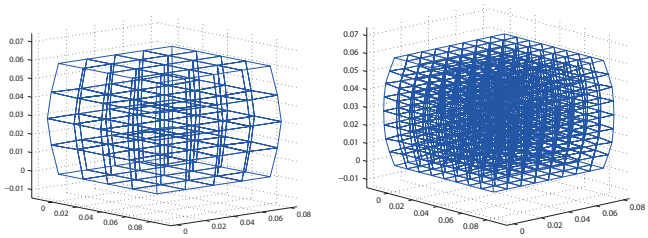

(a) Keep-shape in $5 \times 5 \times 5$ (b) Keep-shape in $9 \times 9 \times 9$

Fig. 5: 3D simulation snapshots for both resolutions.

complicated because the connection matrices are no longer related with the coordinates of nodes. Because less number of elements are involved in square or cubic meshes, computation costs were significantly reduced comparing with triangular and tetrahedra meshes. We found that the speed-up ratios in computation costs are about 30% in 2D and 50% in 3D models respectively and they were not affected much by the nodal resolutions. Comparisons of simulation results between different meshes showed good agreements in deformation but certain differences in rheological forces. However, the force trends were the same which guaranteed the same abilities of both meshes for simulating certain rheological behaviors. After performing model calibration or parameter estimation, the FE models formulated with square or cubic finite elements can work as well as models with triangular or tetrahedra elements for simulating rheological objects.

In the future, parameter estimation for FE models with square or cubic finite elements will be investigated as we have done for the triangular and tetrahedra elements. FE model based on nonlinear Green strain tensor will be also formulated using square and cubic finite elements to simulate large deformation and deformation with rotation motion. Model with irregular shaped objects and contact interaction will also be formulated based on square and cubic elements.

ACKNOWLEDGMENT

This work was supported in part by Grant in Aid for Scientific Research (No. 2324604) and R-GIRO program of Ritsumeikan University.

REFERENCES

[1] M. Hrapko, J.A.W. van Dommelen, G.W.M. Peters, and J.S.H.M. Wismans, "The mechanical behaviour of brain tissue: Large strain response and constitutive modelling", *Biorheology*, vol. 43, pp. 623–636, 2006.

[2] D. Terzopoulos and K. Fleischer, "Modeling inelatic deformation: viscoelasticity, plasticity, fracture", *Proc. 15th Annual Conference on Computer Graphics and Interactive Techniques (SIGGRAPH 1988)*, pp. 269–278, Atlanta, 1988.

[3] N. Sakamoto, M. Higashimori, T. Tsuji, and M. Kaneko, "An optimum design of robotic hand for handling a visco-elastic object based on Maxwell model," *Proc. IEEE International Conference on Robotics and Automation (ICRA2007)*, pp. 1219–1225, Roma, 2007.

[4] G. Bianchi, B. Solenthaler, G. Székely, and M. Harders, "Simultaneous topology and stiffness identification for mass-spring models based on FEM reference deformations," *Proc. 7th International Conference on Medical Image Computing and Computer-Assisted Intervention (MICCAI2004)*, pp. 293–301, Rennes·Saint-Malo, 2004.

[5] H. Yoshida, Y. Murata, and H. Noborio, "A smart rheologic MSD model pushed/calibrated/evaluated by experimental impulses," *Proc. IEEE/RSJ International Conference on Intelligent Robots and Systems (IROS2005)*, pp. 269–276, Edmonton, 2005.

[6] R. Nogami, H. Noborio, S. Tomokuni, and S. Hirai, "A comparative study of rheology MSD models whose structures are lattice and truss," *Proc. IEEE/RSJ International Conference on Intelligent Robots and Systems (IROS2004)*, pp. 3809–3816, Sendai, 2004.

[7] T. Ikawa and H. Noborio, "On the Precision and Efficiency of Hierarchical Rheology MSD Model," *Proc. IEEE/RSJ International Conference on Intelligent Robots and Systems (IROS2007)*, pp. 376–383, San Diego, 2007.

[8] Z. Wang, K. Namima, and S. Hirai, "Physical parameter identification of rheological object based on measurement of deformation and force," *Proc. IEEE International Conference on Robotics and Automation (ICRA2009)*, pp. 1238–1243, Kobe, 2009.

[9] Z. Wang and S. Hirai, "Modeling and parameter identification of rheological object based on FE method and nonlinear optimization," *Proc. IEEE/RSJ International Conference on Intelligent Robots and Systems (IROS2009)*, pp. 1968–1973, St. Louis, 2009.

[10] Z. Wang and S. Hirai, "Modeling and property estimation of Japanese sweets for their manufacturing simulation," *Proc. IEEE/RSJ International Conference on Intelligent Robots and Systems (IROS2010)*, Taipei, 2010, pp. 3536–3541, Taipei, 2010.

[11] Z. Wang and S. Hirai, "Contact modeling and parameter switching for simultaneous reproduction of rheological force and deformation," *Proc. IEEE International Conference on Robotics and Biomimetics (ROBIO2010)*, pp. 726–731, Tianjin, 2010.

[12] Z. Wang and S. Hirai, "Green Strain Based FE Modeling of Rheological Objects for Handling Large Deformation and Rotation," *Proc. IEEE International Conference on Robotics and Automation (ICRA2011)*, pp. 4762–4767, Shanghai, 2011.

[13] J. Baumgarte, "Stabilization of Constraints and Integrals of Motion in Dynamical Systems," *Computer Methods in Applied Mechanics and Engineering*, vol.1, no.1, 1972, pp. 1-16.